Effect of Simulated Welding Cycles on Carbide Evolution in SQV-2A Low Alloy Steel

Jozef JANOVEC*, Makoto TAKAHASHI, Toshio KURODA*** and Kenji IKEUCHI******

Abstract

The influence of simulated welding cycles on the evolution of carbides in SQV-2A low alloy steel was studied. In the investigation TEM observations of thin foils and carbon extraction replicas were performed. Type and metal composition of carbide particles were determined by means of electron diffraction and EDX. In original and "affected" states Fe-rich M_3C and Mo-rich M_2C carbides were identified. The M_2C carbide was found to incur only small changes during simulated welding cycles. There was confirmed a higher sensitivity of M_3C carbide on short-term high-temperature welding processes.

KEY WORDS: (Low Alloy Steels) (Simulating of Welding Cycles) (Carbide Evolution) (TEM) (EDX) (Electron Diffraction)

1. Introduction

The morphology, size, and distribution of secondary phase particles in microstructure significantly influences the mechanical, fracture, and physical properties of alloy steels[1,2]. Segregation phenomena and corrosion resistance are mainly affected by the partitioning of alloying and impurity elements between secondary phase and matrix[3,4]. Thus, the understanding of secondary phase evolution during processing (technological operations) and service seems to be necessary for the achievement of improved properties and higher service reliability of alloy steels.

In low alloy steels of industrial production, carbides are the most important secondary phase. As mentioned above, the evolution of carbide particles is connected with changes in their morphology, size, distribution, crystal structure, and metal composition. The last two changes appear mostly during long-term service[5,6]. They tend towards an equilibrium, and therefore both experimental measurements and thermodynamic calculations should be used in the investigation of carbide evolution[6,7]. On the other hand, technological operations can be mostly characterized as time-limited non-equilibrium processes. The non-equilibrium evolution of carbides (e.g. during welding) is a largely unexamined process and requires the use of experimental techniques like TEM, EDX, and FIM in its investigation.

Depending upon maximum temperature, holding time, and cooling rate of the welding cycle, carbide particles in "affected" low alloy steel can either dissolve themselves (this process must not be completed) or precipitate (this process is usually followed by growth of particle). Cementite particles have tendency to form before precipitation of special carbides or other types of secondary phases[8]. However, Magula and Janovec[9] have reported the preferential precipitation of Mo-rich particles in Cr-Mo-V low alloy steel affected by a simulated welding cycle with a maximum temperature 993 K and Mandziej[10] has observed the precipitation of fine nitride particles in welds of low-carbon steel with higher nitrogen content.

The present work is aimed at the investigation of carbide evolution in SQV-2A low alloy steel affected by three simulated welding cycles (austenitizing, reheating, and tempering). The achieved results are expected to supplement earlier findings concerning the formation and decomposition of M-A constituent in the investigated steel[11,12].

2. Experimental procedure

Samples of 11x11x55 mm with the longer side parallel to the rolling direction were machined from industrially produced sheets of the investigated SQV-2A low alloy steel (for steel chemical composition see **Table 1**). After rolling

† Received on May 31, 2001
* Visiting Research Scholar, (Professor of Inst. of Mat. Res., Slovak Academy of Sciences)
** Reseach Associate
*** Associate Professor
**** Professor
Transactions of JWRI is published by Joining and Welding Research Institute of Osaka University, Ibaraki, Osaka 567-0047, Japan.

Table 1 Chemical composition of the investigated steel (mass contents in %).

Element	C	Si	Mn	P	S	Ni	Mo	Cr	Al
Content	0.18	0.28	1.45	0.005	0.002	0.7	0.54	0.09	0.018

Table 2 Parameters for simulated welding cycles. Terms $t_{8/5}$ and $t_{8/5eff}$ represent the cooling time from 1073 to 773 K. The simulations consisted of one (for denotation of corresponding state symbol **C** was used), two (**A** and **B**), or three (**A1**–**A3** and **B1**–**B3**) cycles.

1st cycle	2nd cycle	3rd cycle	Symbol
1623 K / 6 s, $\Delta t_{8/5}$ = 6 s	- - -	- - -	**C**
1623 K / 6 s, $\Delta t_{8/5}$ = 6 s	1073 K / 6 s, $\Delta t_{8/5}$ = 6 s	- - -	**A**
	1073 K / 6 s, $\Delta t_{8/5}$ = 40 s		**B**
1623 K / 6 s, $\Delta t_{8/5}$ = 6 s	1073 K / 6 s, $\Delta t_{8/5}$ = 6 s	473 K / 6 s, $\Delta t_{8/5eff}$ = 6 s	**A1**
		733 K / 6 s, $\Delta t_{8/5eff}$ = 6 s	**A2**
		893 K / 6 s, $\Delta t_{8/5eff}$ = 6 s	**A3**
1623 K / 6 s, $\Delta t_{8/5}$ = 6 s	1073 K / 6 s, $\Delta t_{8/5}$ = 40 s	473 K / 6 s, $\Delta t_{8/5eff}$ = 6 s	**B1**
		733 K / 6 s, $\Delta t_{8/5eff}$ = 6 s	**B2**
		893 K / 6 s, $\Delta t_{8/5eff}$ = 6 s	**B3**

and before simulation of welding cycles, the steel was normalized at 1153 K for 13.63 ks, water quenched, tempered at 953 K for 24.36 ks, and air cooled. The mentioned heat treatment led to the formation of the original state, symbolised **OR**. Parameters of welding cycles corresponding to austenitizing (1st cycle), intercritical reheating (2nd cycle) and tempering (3rd cycle) are scheduled in **Table 2**. The microstructures of original and "affected" states were observed by light microscopy after two-step electrolytic etching.

To identify phases present in the investigated steel, TEM of carbon extraction replica and thin foil was used. Carbon extraction replicas were removed electrolytically in a solution of HCl (10 ml) in ethylalcohol (100 ml) at room temperature and voltage 12.5 V. Thin foils were also prepared electrolytically in a solution of $HClO_4$ (10 ml) in

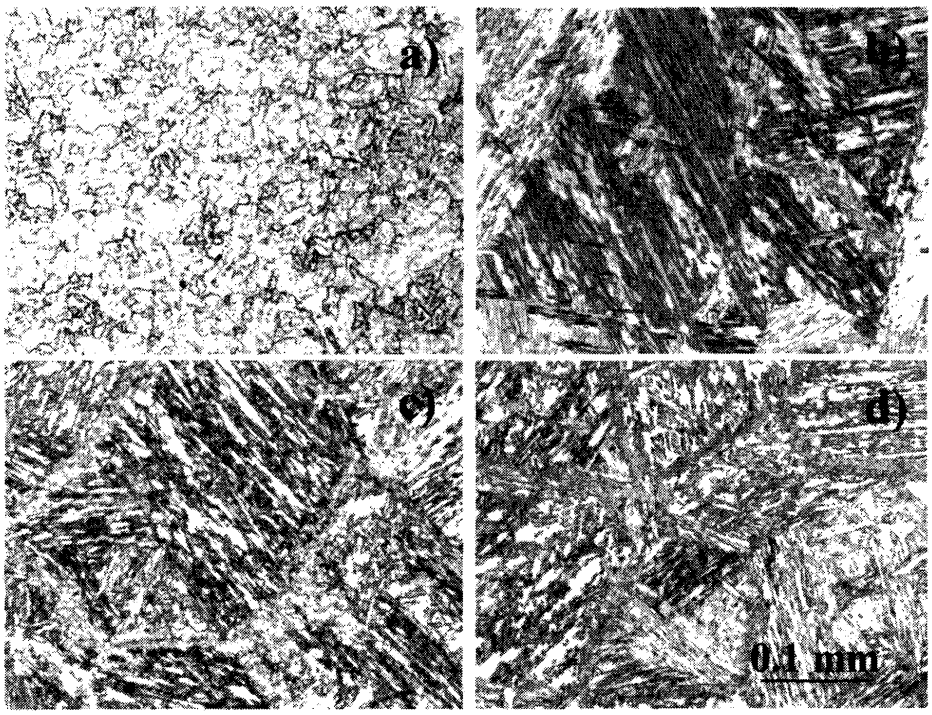

Figure 1 Characteristic microstructures of the investigated steel:
(a) after rolling, normalizing and tempering (**OR**), (b) after 1st welding cycle (state **C**), (c) after 2nd welding cycle (state **A**), (d) after 3rd welding cycle (state **A3**).

ethylenglycolmonobutylether (90 ml) at 288 K and voltage 22 V. Extracted carbide particles were analyzed by means of CBD, SAD and EDX techniques. The metal composition of carbides was determined by means of software for thin samples; corrections for absorption and fluorescence were not applied.

3. Results

Microstructure of the investigated steel is documented in **Fig. 1**. The fine-grain ferrite-carbide microstructure of the original state, Fig. 1(a), was changed into coarse-grain martensite microstructure (state **C**) during 1st welding cycle, Fig. 1(b). For the 2nd welding cycle (states **A** and **B**), the formation of martensite-austenite (M-A) constituent in intergranular and interlath areas is characteristic, Fig. 1(c).

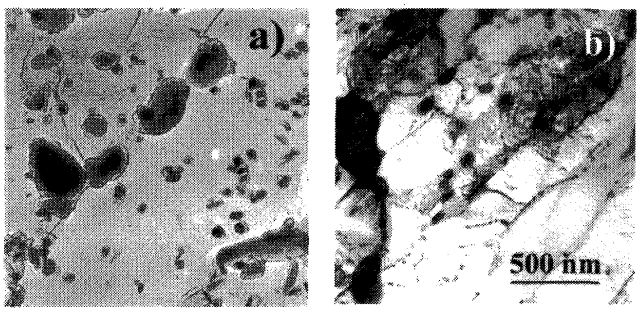

Figure 2 Size, morphology and distribution of carbide particles in the microstructure of original state: (a) TEM micrograph of carbon extraction replica and (b) TEM micrograph of thin foil.

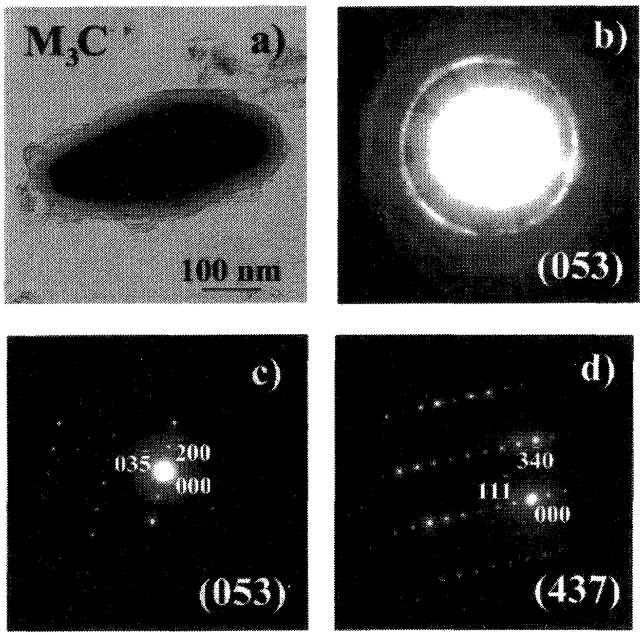

Figure 3 Identification of M_3C carbide by means of electron diffraction: (a) TEM micrograph showing morphology and size of the analyzed particle, (b) Kikuchi lines taken off the particle in orientation (053) by means of convergent beam, (c) SAD pattern of the analyzed particle in orientation (053), (d) SAD pattern of the analyzed particle in orientation (437).

Decomposition of the M-A constituent during 3rd welding cycle did not bring metallographically ascertainable changes in the microstructure, Fig. 1(d).

In the microstructure of the original state carbide, particles of two different types were identified:

- large equiaxed particles (200-500 nm in diameter) at grain and lath boundaries, **Fig. 2**, identified as M_3C carbide, **Fig. 3**,
- small particles (up to 200 nm) of M_2C carbide, **Fig. 4**, precipitating mostly in intralath areas, Fig. 2. Characteristic EDX-spectra of Fe-rich M_3C and Mo-rich M_2C carbides are documented in **Figs. 5**(a) and 5(b), respectively. Crystallographic parameters of both carbides and b.c.c. matrix (a-Fe) are given in **Table 3**.

In the microstructure of state **C** (after 1st cycle) only a

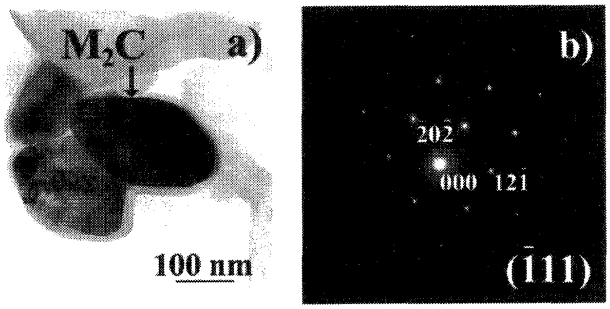

Figure 4 Identification of M_2C carbide by means of electron diffraction: (a) TEM micrograph showing morphology and size of the analyzed particle (marked by arrow), (b) SAD pattern of the analyzed particle in orientation (111).

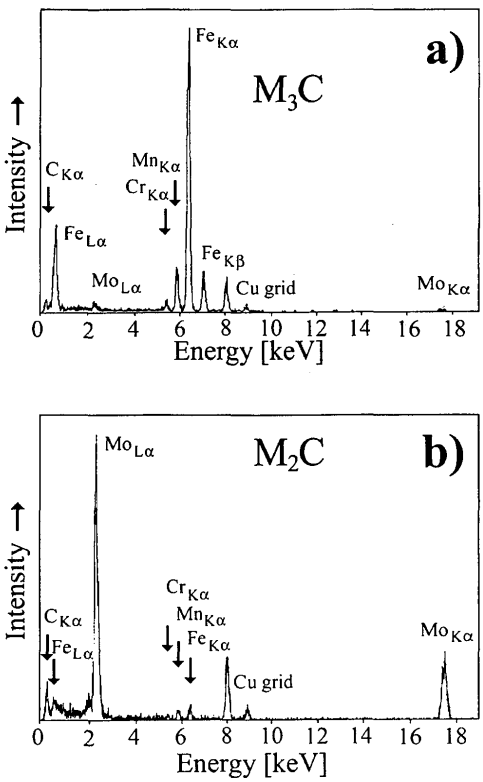

Figure 5 Characteristic EDX-spectra of M_3C (a) and M_2C (b) carbides.

Table 3 Crystallographic parameters of identified phases.

Phase	System	Space group	Lattice parameters [nm]	Reference
M_3C	orthorombic	Pnma	a = 0.50890 b = 0.67433 c = 0.45235	13)
M_2C	hexagonal	$P6_3/mmc$	a = 0.30020 c = 0.47240	14)
α-Fe	b.c.c.	$Im\bar{3}m$	a = 0.28665	13)

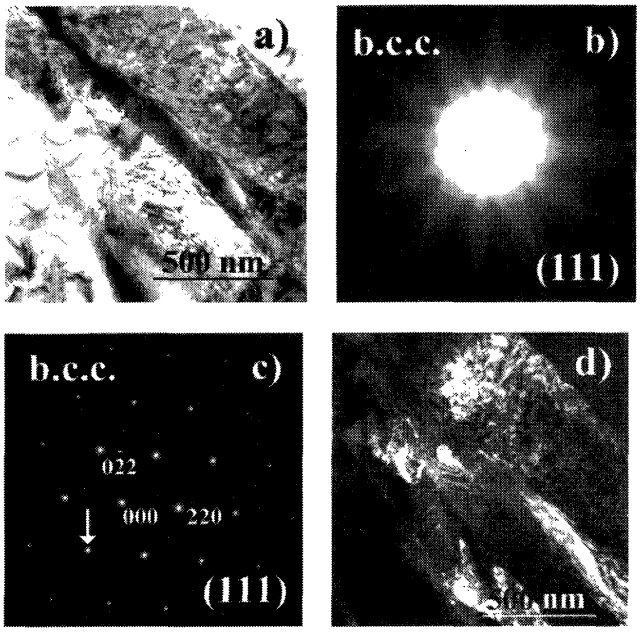

Figure 6 Microstructure of state **A** (1623 K / 6 s, $t_{8/5}$ = 6 s; 1073 K / 6 s, $t_{8/5}$ = 6 s): (a) TEM micrograph showing areas of b.c.c. martensite in M-A constituent practically free of carbide particles, (b) CBD pattern of b.c.c. martensite in orientation (111), (c) SAD pattern in orientation (111) corresponding to the CBD pattern in Fig. 6(b), (d) dark field image taken from the area documented in Fig. 6(a) in reflection signed by arrow in Fig. 6(c).

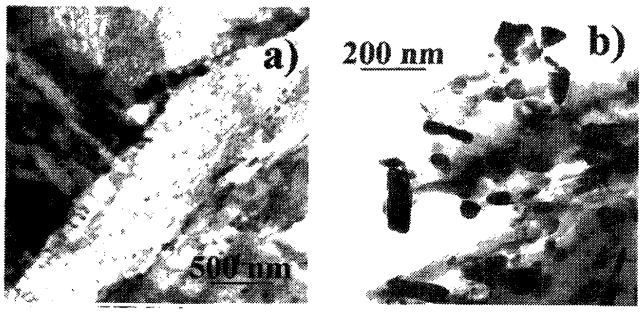

Figure 7 Microstructure of state **B** (1623 K / 6 s, $t_{8/5}$ = 6 s; 1073 K / 6 s, $t_{8/5}$ = 40 s): (a) TEM micrograph showing smaller particles in intralath areas and larger ones along lath boundaries, (b) carbide particles in marginal areas of thin foil visualized by means of TEM.

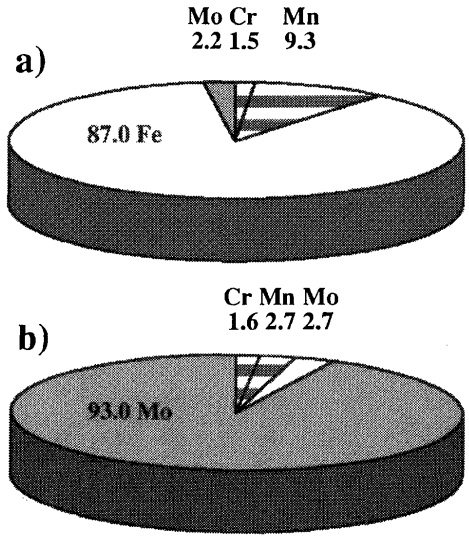

Figure 8 Average atomic contents of Cr, Mn, Fe, and Mo (in %) in metallic part of M_3C (a) and M_2C (b) carbides.

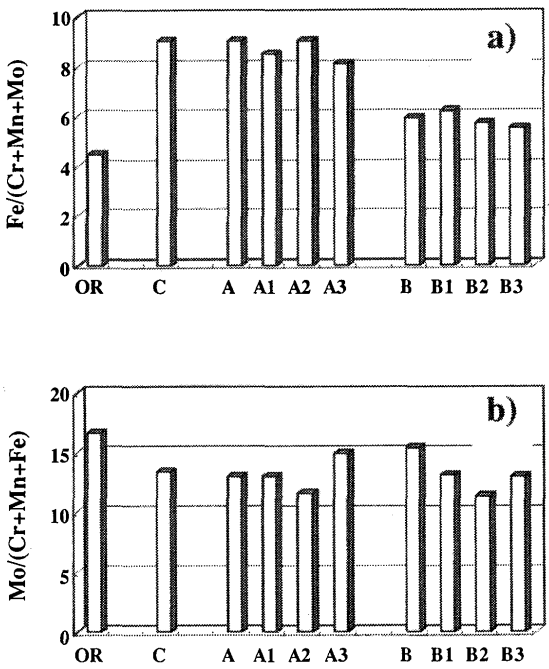

Figure 9 Changes in metal composition of identified carbides (atomic contents of Cr, Mn, Fe, and Mowere taken into account) in analyzed states: (a) Fe/(Cr+Mn+Mo) ratio for carbide M_3C, (b) Mo/(Cr+Mn+Fe) ratio for carbide M_2C.

few carbide particles were observed. They were fine particles of undissolved M_2C carbide and needle-shape M_3C particles of self-tempered martensite. The state of precipitation after the 2nd welding cycle was strongly influenced by the cooling rate of the cycle:

- the microstructure of state A ($\Delta_{t8/5}$ = 6 s) contains the same types of particles as identified in state **C**; the frequency of their occurrence in the microstructure is very low, **Figs. 6**(a) and 6(d); reflections from carbide particles were not found in diffraction patterns of b.c.c. martensite, Fig. 6(c),
- many interlath and intralaths M_3C particles, **Fig. 7**, were observed in the microstructure of state B ($\Delta_{t8/5}$ = 40 s); particles of M_2C carbide were also found.

Tempering of the investigated steel at 733 and 893 K (3rd welding cycle) led to the additional precipitation and growth of carbide particles. Besides M_3C and M_2C carbides, there were not found any other carbide types.

In the metallic part of both identified carbides, Cr, Mn, Fe, and Mo were found. Average contents of mentioned elements in M_3C and M_2C carbides are illustrated in **Figs. 8**(a) and 8(b), respectively. Changes in metal composition of identified carbides evoked by simulated welding cycles are plotted in **Fig. 9**. For the M_3C carbide the ratio Fe/(Cr+Mn+Mo), Fig. 9(a), and for the M_2C carbide the ratio Mo/(Cr+Mn+Fe), Fig. 9(b), were chosen to reflect the mentioned changes.

4. Discussion

In all analyzed states the same carbide types (M_3C and M_2C) were found. Differences between individual states are only in morphology, area density, distribution and metal composition of carbide particles. Time-temperature parameters of welding cycles (short-term holding at maximum temperature and relatively fast cooling) supported the dissolving of carbide particles rather than their precipitation and growth. This is the reason why the area density of carbide particles in "affected" states is evidently lower than in the original state. There are also differences between original and "affected" states in the bulk distribution of carbon. In the original state, the even distribution of carbon led to the equable distribution of carbide particles. Reaustenitizing during the 2nd welding cycle accompanied by partitioning of carbon between ferrite and austenite caused the enrichment of austenite (after cooling M-A constituent) with carbon. Okada et al.[15] have reported for steels HT80-A, HT80-B, and HT100-B that the carbon content in M-A constituent can be even 20x higher than in the surrounding ferrite. This is also the reason why precipitation of carbide particles in "affected" states took place preferentially in islands of M-A constituent (gray areas along grain and lath boundaries in Figs. 1(c) and 1(d)).

4.1. Carbides in original state

As already mentioned in previous paragraphs the microstructure of the original state consists of ferrite, cementite or ε-carbide (the term M_3C was used because of a prevalence of cementite particles), and M_2C carbide. Particles of both carbide types are uniformly distributed in the microstructure, even if evidently larger M_3C particles are mostly situated along grain boundaries, Fig. 2. Molybdenum in M_2C carbide of the original state is the dominant metallic element which is evident from the value of about 16 of the Mo/(Cr+Mn+Fe) ratio, Fig. 9(b). Only traces of Cr, Mn, and Fe were found in this carbide, Fig. 5(b). Fe-rich M_3C carbide was also found to be alloyed by Mn (atomic content about 10 %), Fig. 8(a); atomic contents of Cr and Mo are under 2.5 %.

4.2. Carbide evolution during simulated welding cycles

Dissolving of carbide particles is the decisive process occurring in the investigated steel during the 1st welding cycle. Differences in metal composition of M_3C carbide before (**OR**) and after (**C**) simulation, Fig. 9(a), indicate that cementite of the original state should be completely dissolved during holding at 1623 K for 6 s and ε-carbide reprecipitates later as a part of self-tempered martensite; a higher Fe-content is characteristic for the "fresh" cementite (ε-carbide). In low alloy steels "freshly" precipitated M_2C particles are mostly of needle-shape morphology[16]. In state **C** fine (up to 50 nm in diameter) M_2C particles of equiaxed morphology were observed and metal composition comparable with particles of the same carbide in state **OR**, Fig. 9b. This indicates the M_2C carbide was partially (incompletely) dissolved during the 1st welding cycle, while new M_2C particles did not precipitate.

As documented in Figs. 6(a) and 7(a), cooling rate exerted a significant influence on the carbide evolution during the 2nd welding cycle. In the microstructure of faster cooled ($\Delta_{t8/5}$ = 6 s) state **A** only fine cementite (ε-carbide) particles of self-tempered martensite, Fig. 6(a), were found. Not only morphology, but also metal composition of these particles is comparable with those in state **C**. Slower cooling ($\Delta_{t8/5}$ = 6 s) made possible intensive precipitation of interlath and intralath M_3C particles, Fig. 7. They are evidently smaller than M_3C particles in the original state (compare Fig. 7(a) with Fig. 2(b)), but differences in metal composition become smaller, Fig. 9(a). The value of the Fe/(Cr+Mn+Mo) ratio decreases and the stability of M_3C carbide increases in accordance with sequence:

C, A, A1-A3 > B, B1-B3 > OR.

No changes in morphology and metal composition of M_2C carbide were detected during 2nd welding cycle, Fig. 9(b).

The state of precipitation formed during 2nd welding cycle was also maintained during the 3rd welding cycle. At

higher temperatures 733 and 893 K additional precipitation and growth of M_3C particles were observed. Precipitation of M_2C particles was not experimentally detected, even if it can be possible. Changes in metal composition of both carbides as a function of the 3rd cycle maximum temperature are negligible, Fig. 9.

The achieved results confirmed that in the investigated steel the M_3C carbide is more sensitive to short-term high-temperature changes evoked by simulated welding cycles than M_2C carbide. More significant changes in the occurrence, morphology and metal composition were detected for the former carbide only.

4.3. Practical aspects of carbide evolution

In the previous paper[17] the relationship between parameters of simulated welding cycles and values of absorbed energy (achieved by Charpy impact test at 293 K) was discussed. Absorbed energies for states **A** and **A1** - **A3** were higher than for states **B** and **B1** - **B3**, respectively. After the 3rd welding cycle the local maximum of absorbed energy was recorded at temperature 733 K (states **A2** and **B2**). This indicates that not only formation of M-A constituent[11,12], but also precipitation of M_3C particles in C-rich M-A islands evokes the reduction of absorbed energy in the investigated steel. The decrease in hardness HV 10 of M-A islands with increasing maximum temperature of the 3rd cycle, Fig. 10, is a consequence of microstructure changes including the growth of carbide particles[17]. Hardness HV 10 of the ferrite matrix is practically constant, **Fig. 10**, which indicates negligible carbide changes outside of the M-A constituent. The presented knowledge is progressive from the welding parameter optimizing point of view.

5. Conclusions

The results of carbide evolution in SQV-2A low alloy steel during simulated welding cycles can be summarize as follows:

(1) In the original and "affected" states the Fe-rich M_3C carbide and Mo-rich M_2C carbide were identified.

(2) Besides Fe and Mo, Cr and Mn were also found in the metallic part of both identified carbides.

(3) The M_2C carbide was found to incur only small changes during simulated welding cycles, except the drastic reduction of its appearance in the microstructure during the 1st cycle.

(4) There were observed repeated dissolutions and precipitations (growths) of M_3C particles during simulated welding cycles accompanied by changes in the carbide metal composition. It was confirmed that a higher sensitivity of this carbide to short-term high-temperature processes typical for welding existed.

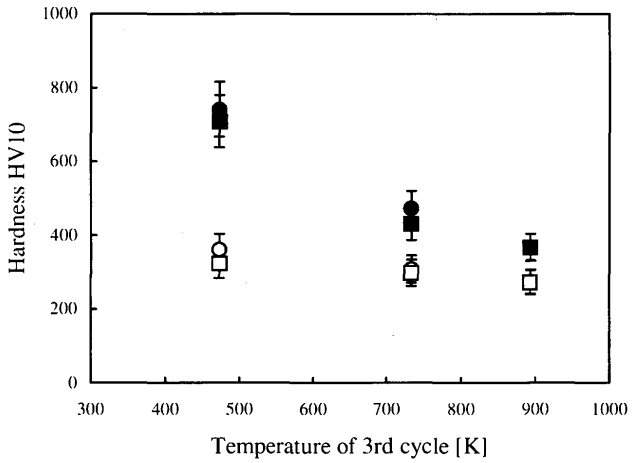

Figure 10 Hardness HV 10 of M-A constituent (● - state **A**, ■ - state **B**) and ferrite matrix (○ - state **A**, □ - state **B**) as a function of 3rd cycle maximum temperature.

(5) It was shown that not only formation of M-A constituent, but also precipitation of M_3C particles evoke the reduction of absorbed energy in the investigated steel.

References

1) S. Wignarajah, I. Masumoto and T. Hara: ISIJ Int., **30** (1990), 58.
2) J. Janovec: Grain Boundary Segregation, Secondary Phase Precipitation and Intergranular Embrittlement of Alloy Steels, Dr.Sc. thesis, Slovak Academy of Sciences – Institute of Materials Research, Kosice, (1997).
3) J. Janovec, A. V_rostková, J. Perhácová, V. Homolová, H. J. Grabke, P. Sevc and M. Lucas: Steel Res., **70** (1999), 267.
4) R. Beltran, J. G. Maldonado, L. E. Murr and W. W. Fischer: Acta Mater., **45** (1997), 4351.
5) J. Janovec, A. V_rostková and A. Hol_: J. Mater. Sci., **27** (1992), 6564.
6) A. V_rostková, A. Kroupa, J. Janovec and M. Svoboda: Acta Mater., **46** (1998), 31.
7) A. Kroupa, A. V_rostková, M. Svoboda and J. Janovec: Acta Mater., **46** (1998), 39.
8) J. Janovec, V. Magula and A. Hol_: Kovové Mater., **30** (1992), 44.
9) V. Magula and J. Janovec: Ironmaking and Steelmaking, **21** (1994), 223.
10) S. T. Mandziej: Scripta Metall. Mater., **27** (1992), 793.
11) K. Ikeuchi, J. Liao, H. Tanabe and F. Matsuda: ISIJ Int., (1995), 1203.
12) F. Matsuda, Y. Fukada, H. Okada, Ch. Shiga, K. Ikeuchi, Y. Horii, T. Shiwaku and S. Suzuki: Weld. World, **37** (1996), 134.
13) P. Villars and L. D. Calvert: Pearson's Handbook of Crystallographic Data for Intermetallic Phases, 1st edition, Ohio, ASM, (1985).
14) K. W. Andrews, D. J. Dyson and S. R. Keown: Interpretation of Electron Diffraction Pattern, Adam Hilger, London, (1971).
15) H. Okada, K. Ikeuchi, F. Matsuda, I. Hrivnak and Z. Li: Quarterly J. Japan Weld. Soc., **12** (1994), 236.
16) B. A. Senior: Mater. Sci. Eng., **A103** (1988), 263.
17) J. Janovec, M. Takahashi, T. Kuroda and K. Ikeuchi: ISIJ Int., **40-Sup.** (2000), S44.